



# Pd-doped organosilica membrane with enhanced gas permeability and hydrothermal stability for gas separation

Huating Song<sup>1</sup>, Shuaifei Zhao<sup>1,2,\*</sup>, Jiaojiao Lei<sup>1</sup>, Chenying Wang<sup>1</sup>, and Hong Qi<sup>1,\*</sup>

<sup>1</sup> State Key Laboratory of Material-Oriented Chemical Engineering, Membrane Science and Technology Research Center, Nanjing Tech University, Nanjing 210009, Jiangsu, China

<sup>2</sup> Faculty of Science and Engineering, Macquarie University, Sydney, NSW 2109, Australia

Received: 15 December 2015

Accepted: 23 March 2016

Published online:

1 April 2016

© Springer Science+Business Media New York 2016

## ABSTRACT

A Pd-doped organosilica membrane based on bis(triethoxysilyl)ethane is successfully developed by the polymeric sol-gel method. Its microstructure, chemical composition, and separation performance are compared with those of the undoped organosilica membrane. Gas adsorption analysis indicates that the Pd-doped organosilica membrane has larger micropores compared with the undoped organosilica membrane. The gas permeation results show that the Pd-doped organosilica membrane has much higher gas permeances than the undoped organosilica membrane due to the enlarged micropores after Pd-doping. The Pd-doped organosilica membrane also exhibits a significantly improved hydrothermal stability. The enhanced hydrothermal stability can be explained by the mechanism that Pd particles act as inhibitors and prevent the formation of mobile silica groups (e.g., Si-OH) under steam condition. Metal-doping (e.g., Pd-doping in this work) may offer a new approach to develop high performance membranes with enhanced gas permeances and hydrothermal stabilities in gas separation applications.

## Introduction

Membrane separation is one of the most cost-effective and promising technologies for various gas separation applications, such as hydrogen recovery, carbon dioxide separation, and air separation [1, 2]. Compared with conventional gas separation methods, such as cryogenic distillation, adsorption, and absorption, membrane gas separation has the advantages of small

footprint, ease of operation, low energy consumption, and low investment cost [1, 3–5].

At present, separation of hydrogen (H<sub>2</sub>) from carbon dioxide (CO<sub>2</sub>) is of particular interest for membranologists as it could address the global issues related to both energy security (via hydrogen production) and climate change (via pre-combustion carbon capture) [3, 6, 7]. In recent years, considerable efforts have been made to develop inorganic

Address correspondence to E-mail: zhassy001@mymail.unisa.edu.au; shuaifei.zhao@mq.edu.au; hqi@njtech.edu.cn

membranes for H<sub>2</sub> separation [3]. Inorganic membranes generally have excellent resistance to high temperature and high pressure [8].

Amorphous microporous silica membranes have received a great deal of attention in gas separation, particularly in separation of gas pairs like H<sub>2</sub>/N<sub>2</sub>, H<sub>2</sub>/CH<sub>4</sub>, H<sub>2</sub>/CO, and H<sub>2</sub>/CO<sub>2</sub>, since silica is an excellent inorganic material with amorphous structures containing irregular pores with a mean size of ~3 Å [8]. The microporous structures of silica membranes in sub-nanometer scales can be precisely controlled by the sol–gel method and calcination [9, 10]. Therefore, silica membranes with excellent permeability and permselectivity can be fabricated. These silica membranes can be employed in harsh environments, such as high pressure and elevated temperature conditions. These characteristics of silica membranes make them promising in hydrogen recovery and pre-combustion CO<sub>2</sub> capture [8, 11–13].

However, pure silica membranes cannot maintain structural stabilities in the presence of water vapor [14]. Namely, they suffer from dissociation of siloxane groups (i.e., hydrolysis of Si–O–Si groups) due to hydrothermal activity. As a result of hydrolysis, mobile silanol groups generate and condense at higher-attraction-energy regions in smaller pores, leading to pore closure. Prolonged exposure to water vapor can also result in large non-selective pores [15, 16]. To improve the hydrothermal stability of silica membranes, three strategies have been proposed. The first approach is the modification of silica membranes using hydrophobic groups to protect siloxane bonds from water by the shield effect [17, 18]. The second method is doping metal (e.g., Ni, Co, Zr, Ti, and Nb) into the silica matrix [19–24]. Metal ions then incorporate into the silica network or metal particles disperse into the silica matrix. The resultant M–O–Si (M for metal) structure or membrane matrix shows outstanding stability in water steam. The third strategy is the development of inorganic–organic hybrid silica membranes instead of pure silica membranes. The hybrid silica membranes contain organic linking groups that confer essential stability for the membranes in the presence of water steam [15, 25, 26].

Ethane-bridged organosilica, i.e., 1,2-bis(triethoxysilyl)ethane (BTESE), has been widely used to develop hybrid organic–inorganic silica membranes [27–31]. Qureshi et al. [31] reported a defect-free composite membrane with a homogeneously ethane-bridged organosilica separation layer. Effects of the operational

parameters in the sol–gel process on the membrane performance were systematically investigated. Under optimal fabrication conditions, the derived organosilica membrane had a hydrogen permeance of  $2.7 \times 10^{-7}$  mol m<sup>-2</sup> s<sup>-1</sup> Pa<sup>-1</sup>, and H<sub>2</sub>/CO<sub>2</sub>, H<sub>2</sub>/N<sub>2</sub> and H<sub>2</sub>/CH<sub>4</sub> permselectivity of 5.8, 21, and 24, respectively.

To improve the gas separation performance of organosilica membranes, an effective approach is to incorporate metals into the organosilica matrix. Nb- and Zr-doped organosilica membranes have been reported by Qi et al. [32] and ten Hove et al. [33]. Due to the denser structures after metal (Nb and Zr) incorporation into the membrane architecture, Nb and Zr-doped organosilica membranes show unprecedented permselectivities. However, the improvement in permselectivity is at the cost of gas permeance loss. Kanezashi et al. [34] developed thin Pd–silica mixed-matrix membrane with improved hydrogen permeability and hydrothermal stability.

In this study, we develop a novel Pd-doped organosilica membrane using BTESE and PdCl<sub>2</sub> as precursors via the sol–gel method. The high dispersion of Pd particles in the organosilica layer was confirmed by X-ray diffractometer (XRD), X-ray photoelectron spectroscopy (XPS) and transmission electron microscopy (TEM). The effects of Pd particles on the microporous structure, chemical composition, gas separation performance, and hydrothermal stability of the organosilica membrane are investigated.

## Experimental

### Sol synthesis and characterization

All chemicals were used as received unless stated otherwise. BTESE (purity = 97 %) from ABCR was used as the organosilica precursor. Palladium chloride (PdCl<sub>2</sub>, purity >98 %, Merger) was selected as the Pd source. Absolute ethanol (EtOH, purity ≥99.9 %) was purchased from Merck. Concentrated chlorhydric acid (HCl, 36.46 wt%) was purchased from Dongfang in China. Acetylacetone (AcAc, in analytical grade) from Lingfeng in Shanghai was selected as the metal complexing agent to stabilize the Pd-doped organosilica (POS) sols.

The following procedure was performed to prepare the organosilica (OS) sols. First, 5 mL BTESE and 5 mL ethanol were mixed in a glove-box under a nitrogen atmosphere. Meanwhile, 5.24 mL chlorhydric acid

solution ( $0.1 \text{ mol L}^{-1}$ ) was prepared by diluting the concentrated chlorhydric acid with deionized water and mixed with 10 mL ethanol in a beaker. The mixture of HCl and ethanol was dropwise added into the BTESE–ethanol mixture under vigorous stirring in an ice bath. Along with continuous stirring, the final mixture was refluxed in a water bath at  $60 \text{ }^\circ\text{C}$  for 90 min. The final molar ratio of the OS sol with respect to BTESE:EtOH:H<sub>2</sub>O:HCl was 1:19.6:22.24:0.2.

POS sols were prepared by the following reaction route. 0.2153 g PdCl<sub>2</sub> was dissolved with 0.27 mL concentrated chlorhydric acid in a water bath at  $60 \text{ }^\circ\text{C}$  for 40 min. Then 15 mL ethanol and 0.125 mL AcAc were added into the PdCl<sub>2</sub>–HCl solution and the mixture was placed in an ice bath. Subsequently, 5.74 mL OS sols (a molar ratio of 1:19.6:11.12:0.1 for BTESE:EtOH:H<sub>2</sub>O:HCl) were added into the mixture under vigorous stirring and reacted at  $60 \text{ }^\circ\text{C}$  for 90 min. The synthesis operations were conducted in a cleaning room. The prepared sol solutions were stored at  $-16 \text{ }^\circ\text{C}$  prior to further use.

The hydrodynamic diameter of freshly synthesized sols was characterized by dynamic light scattering (DLS, Malvern Zetasizer nano ZS90). Prior to measurement, sol solutions were filtered using a filter with a pore size of  $0.2 \text{ }\mu\text{m}$  to remove dusts and clusters.

### Gel preparation and characterization

Dried flake gels were obtained by drying the corresponding sols for 12 h in petri dishes at room temperature. Thermal treatment was conducted after the flakes were ground into powders under reductive atmosphere (i.e., a gas mixture of H<sub>2</sub> and N<sub>2</sub> at a molar ratio of 2:3). This procedure included a heating process with a rate of  $0.5 \text{ }^\circ\text{C min}^{-1}$ , heat preservation for 3 h at  $400 \text{ }^\circ\text{C}$  and subsequently a cooling process with a rate of  $0.5 \text{ }^\circ\text{C min}^{-1}$ .

Crystal structures of the powders were detected by X-ray diffractometer (MiniFlex 600, Rigaku) with a Cu K $\alpha$  radiation at 40 kV and 15 mA. Fourier transform infrared (FTIR) spectroscopy (NICOLET 8700, Thermo Nicolet Corporation) was used to detect the chemical structure of powders calcined at  $400 \text{ }^\circ\text{C}$  with KBr as the reference. X-ray photoelectron spectroscopy measurements for detecting the chemical state of palladium and the chemical structure of the powders were performed on an ESCALAB250xi spectrometer (Thermo Scientific) equipped with a mono-chromatic Al K $\alpha$  X-ray source (1486.6 eV). N<sub>2</sub> and CO<sub>2</sub>

(purity = 99.99 %) from the Nanjing Special Gases Company were used to evaluate the microstructure of the powders via the gas adsorption method. N<sub>2</sub> adsorption–desorption isotherms at 77 K, and H<sub>2</sub>, CO<sub>2</sub>, and CH<sub>4</sub> adsorption isotherms at 298 K were conducted with a physical gas adsorption instrument (ASAP 2020, Micromeritics). The pore size distributions of the powders were obtained from the N<sub>2</sub> adsorption–desorption isotherms based on a cylindrical pore model. Prior to the measurements, samples were degassed under vacuum at 373 K for 12 h. Microstructures of the powders were observed by transmission electron microscopy (JEM-200CX, JEOL).

### Membrane preparation and characterization

OS and POS sols were diluted to the same Si concentration ( $0.17 \text{ mol L}^{-1}$ ) and then were used for dip-coating on  $\gamma\text{-Al}_2\text{O}_3$  mesoporous membranes (pore diameter of 3–5 nm). To avoid the effect of dusts, coating was performed under clean room condition and the diluted sol solutions were filtered using a filter with a pore size of  $0.2 \text{ }\mu\text{m}$ . Subsequently, the membranes were dried for 3 h in an oven with constant temperature and humidity. Prepared membranes were thermally treated by the procedure described in “Gel preparation and characterization” section.

Single gas permeation and hydrothermal stability tests were conducted with a dead-end setup (Fig. 1). Gas permeances of the OS membrane and POS membrane were measured at  $200 \text{ }^\circ\text{C}$  under a transmembrane pressure of 0.3 MPa. Membranes were tested using various gases with different kinetic diameters ( $d_k$ ), including He ( $d_k = 2.55 \text{ \AA}$ ), H<sub>2</sub> ( $d_k = 2.89 \text{ \AA}$ ), CO<sub>2</sub> ( $d_k = 3.3 \text{ \AA}$ ), N<sub>2</sub> ( $d_k = 3.64 \text{ \AA}$ ), CH<sub>4</sub> ( $d_k = 3.8 \text{ \AA}$ ), and SF<sub>6</sub> ( $d_k = 5.5 \text{ \AA}$ ). The gas permselectivity (i.e., ideal selectivity) was equal to the permeance ratio between two gases.

Hydrothermal stabilities of the membranes were evaluated by measuring the single gas permeances before and after in situ exposure to a mixture of N<sub>2</sub> and steam. Steam was generated with a steam generator and mixed with N<sub>2</sub>. N<sub>2</sub> pressure was maintained at 0.3 MPa with a pressure gauge. Water vapor pressures were controlled between 8 and 100 kPa by adjusting the steam temperatures (at 41.3, 53.5, 66.5, 75, 85.6, and 99.6  $^\circ\text{C}$ , and the corresponding vapor pressures were 8, 15, 30, 40, 60, and 100 kPa, respectively). After hydrothermal treatment, membranes were dried for 2 h with a N<sub>2</sub> sweep at the

**Figure 1** Schematic representation of the experimental apparatus for single gas permeation and hydrothermal stability tests. 1 stop valve, 2 pressure gauge, 3 steam generator, 4 three-way valve, 5 electric furnace, 6 membrane module, 7 membrane, 8 O-ring, 9 gas washing bottle, 10 soap-film flow meter.

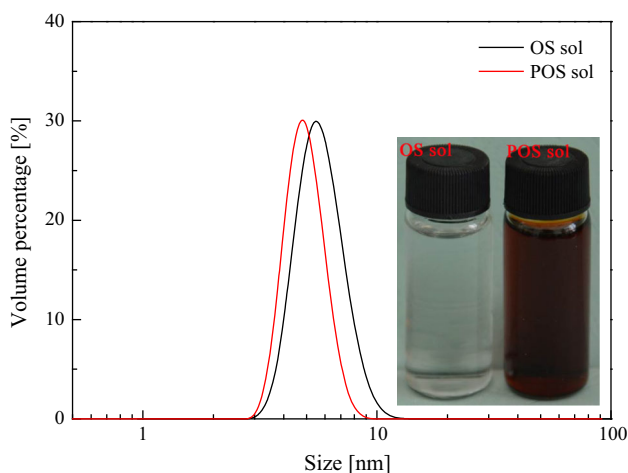
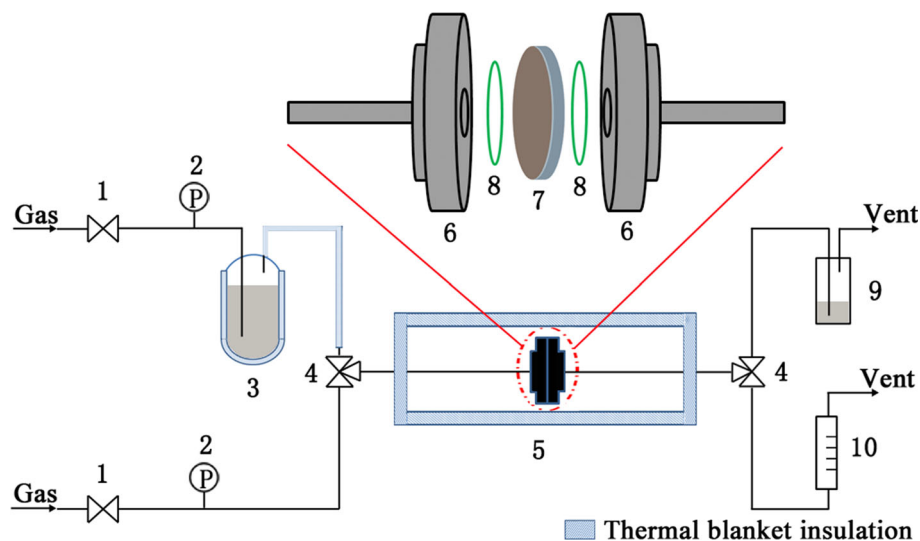


**Figure 2** Particle size distributions of the organosilica (OS) and Pd-doped organosilica (POS) sols. Inset photographs of the two types of sols.

same temperature (i.e., 200 °C). Single gas permeation tests were then performed as described above.

## Results and discussion

### Sol characteristics

Figure 2 describes the particle size distributions of the OS and POS sols. Particle size distributions are within 3–9 and 3–12 nm, and the mean particle sizes are 4.8 and 5.4 nm for the OS sol and POS sol, respectively. The inset in Fig. 2 shows the appearance of the OS and POS sols. Homogeneous sols were obtained by the polymeric sol–gel route. The OS sol is

clear and transparent, while the POS sol is reddish brown, similar to the color of the palladium chloride solution. No agglomerations were observed during preservation at  $-16$  °C. Thus, we selected the homogenous and stable OS sol and POS sol with similar size distributions to fabricate membranes.

The prepared OS and POS sols have high quality for membrane fabrication, which is confirmed by the excellent molecular sieving properties of the OS membrane and POS membrane as reported following.

### Gel characteristics

#### Chemical state of palladium

XRD patterns of the OS powders and POS powders calcined at 400 °C (Fig. 3) show that no diffraction peaks for OS powders, suggesting a disordered or amorphous structure in the unsupported OS membrane. Diffraction peaks of zero valent Pd ( $2\theta = 40.14^\circ$ ,  $46.70^\circ$ , and  $68.18^\circ$ ) were detected, whereas no diffraction peaks of crystalline  $\text{SiO}_2$  were observed in the POS powders. Pd crystal size, calculated by Scherer's equation, was 11.4 nm.

XPS analysis was conducted to better understand the chemical state of palladium. Figure 4 illustrates the XPS spectra of the OS and POS powders calcined at 400 °C. Energy adsorption from Si, C, and O were observed in the XPS spectra of the OS and POS powders. Photoelectron energy adsorption peak from Pd was also detected in the POS powders. Figure 5 shows the XPS spectra of Pd  $3d_{3/2}$  and Pd  $3d_{5/2}$  regions of the POS powders. Core-level peaks at

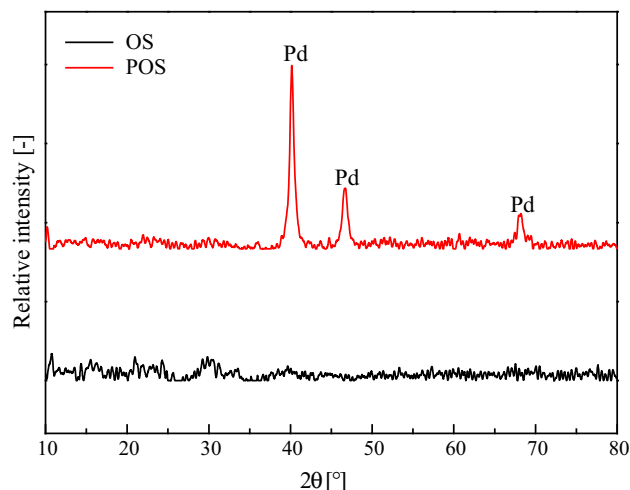


**Figure 3** XRD patterns of the organosilica (OS) and Pd-doped organosilica (POS) powders calcined at 400 °C.

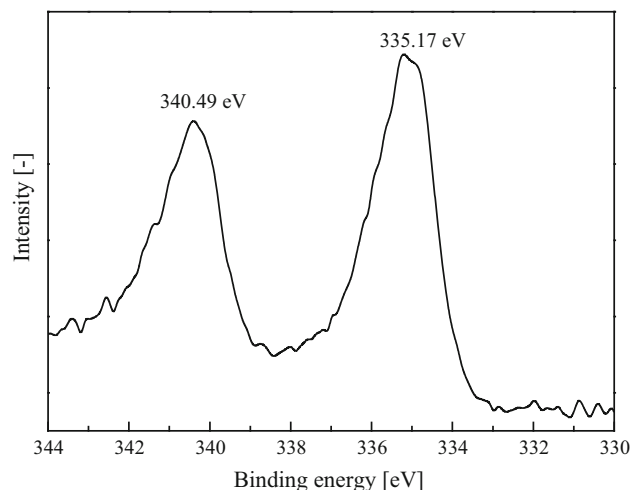


**Figure 5** XPS spectra of the Pd<sub>3/2</sub> and Pd<sub>5/2</sub> regions of the Pd-doped organosilica (POS) powders calcined at 400 °C in a mixture of H<sub>2</sub> and N<sub>2</sub>.

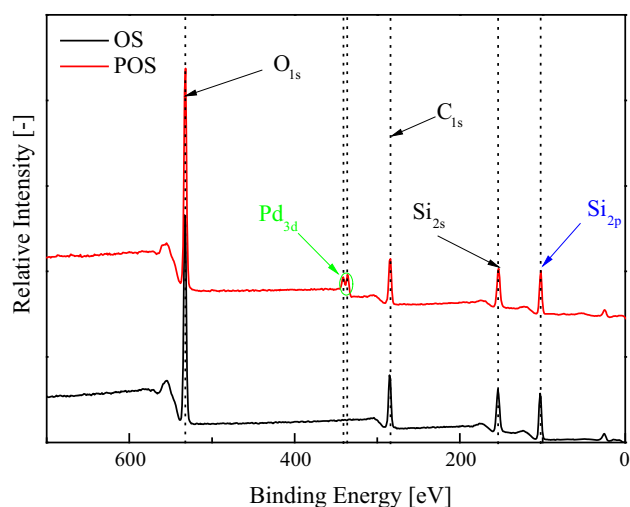


**Figure 4** XPS spectra of the organosilica (OS) and Pd-doped organosilica (POS) powders calcined at 400 °C.

340.49 and 335.17 eV correspond to the 3d<sub>3/2</sub> and 3d<sub>5/2</sub> binding energy peaks of zero valent Pd, respectively. There are no shifts with these two peaks. These results indicate that there are no interactions between the Pd and the organosilica, and that the Pd is not incorporated into the organosilica networks, but may randomly disperse in the POS powders. This assumption is confirmed by TEM characterization (Fig. 6).

Figure 6 shows the TEM images of the OS and POS powders. For the OS powders, amorphous silica was observed, while for the POS powders, Pd particles with sizes of 3–10 nm were well dispersed in the amorphous

organosilica powders. In addition to the particle size of Pd, other relevant parameters such as the ratio of amorphous/crystalline domains and density of particles may also have significant effects on membrane performance. These parameters can be adjusted by the change in experimental conditions (e.g., treatment atmospheres, calcination temperatures, and heating rates). Relevant study will be carried out in the future.

For metals (e.g., Nb, Co, Al, Ni) doped in silica membranes, the chemical state of the metal has a remarkable influence on membrane performance [19, 23, 35]. Metals may have two chemical states in the membranes. First, metals can be covalently linked with siloxane to form M–O–Si networks, leading to denser network structures [36, 37]. Second, metals or metal oxides can disperse in the silica matrix, resulting in hydrostable and highly selective membranes [34, 38]. For the POS unsupported membrane in this work, dispersion of Pd crystals in the organosilica matrix was confirmed on the basis of the TEM results.

### Chemical structure

FTIR spectra of the OS and POS powders calcined at 400 °C (Fig. 7) show conspicuous absorption band at around 1020 cm<sup>-1</sup> that can be attributed to the asymmetric stretching vibration of the Si–O–Si groups [39]. The broad absorption band at 3200–3700 cm<sup>-1</sup> is assigned to the stretching vibrations of hydroxyl groups in Si–OH (absorption peak: 3450 cm<sup>-1</sup>) and

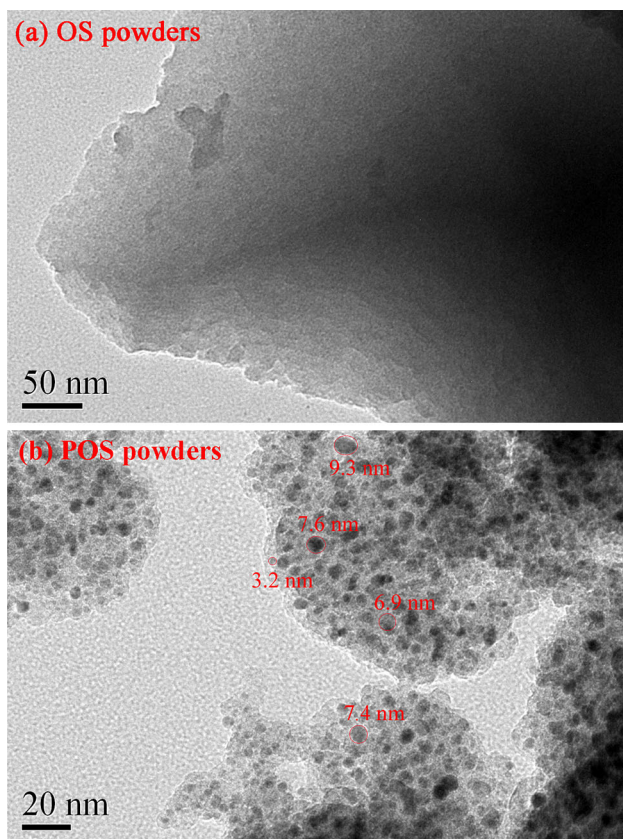


**Figure 6** TEM images of the organosilica (OS) (a) and Pd-doped organosilica (POS) (b) powders calcined at 400 °C.

adsorbed water (absorption peak: 3250  $\text{cm}^{-1}$ ) [39]. Absorption peaks at approximately 2910, 1640, 1410, 1270, 775, and 700  $\text{cm}^{-1}$  can be ascribed to C–H<sub>2</sub> asymmetric stretching, H–O–H (adsorbed water) stretching, CH<sub>2</sub> (in Si–CH<sub>2</sub>–CH<sub>2</sub>–Si) asymmetric bending, CH<sub>3</sub> (in CH<sub>3</sub>–SiO<sub>3/2</sub>) symmetric bending, CH<sub>2</sub> (in –OCH<sub>2</sub>CH<sub>3</sub>) rocking, and Si–C stretching vibrations, respectively [37, 39, 40].

Deconvolutions of XPS Si<sub>2p</sub> peaks from the OS and POS powders (Fig. 8) reveal that core-level spectra can be decoupled into three peaks (103.5, 102.6, and 101.8 eV) with Gaussian contributions corresponding to inorganic moieties (i.e., SiO<sub>4/2</sub> and XSiO<sub>3/2</sub>) and organic moiety (i.e., X<sub>2</sub>SiO<sub>2/2</sub>) [39]. The content of the inorganic moieties is much higher than that of the organic moiety in the OS and POS powders.

Results from FTIR and XPS offer significant insights into the chemical composition of the networks in the prepared membranes. Structural data indicate that Pd particles are randomly dispersed in the organosilica matrix and have no covalent bonds with siloxane.

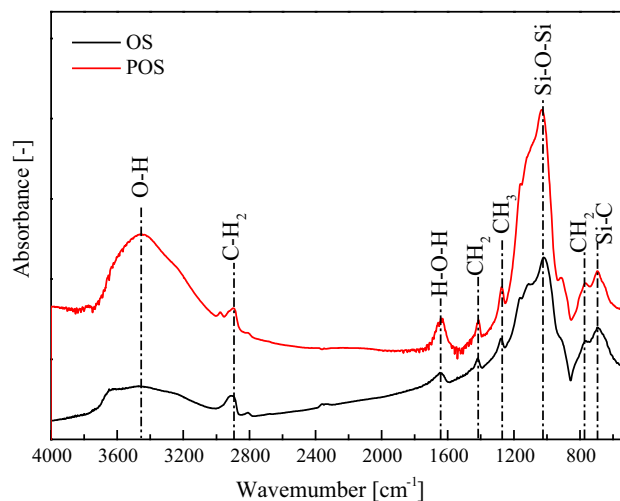


**Figure 7** FTIR spectra of the organosilica (OS) and Pd-doped organosilica (POS) powders calcined at 400 °C.

### Micropore structure

Nitrogen adsorption–desorption measurements were performed to evaluate the micropore structure of the OS and POS unsupported membranes. Figure 9 describes the nitrogen adsorption–desorption isotherms of the POS powders. The type I isotherm, characteristic of typical microporous materials [41], are observed for the two samples. The OS unsupported membrane has a BET surface area of 338  $\text{m}^2 \text{g}^{-1}$  and a pore volume of 0.173  $\text{cm}^3 \text{g}^{-1}$ , while the POS unsupported membrane has a higher BET surface area of 476.8  $\text{m}^2 \text{g}^{-1}$  and a larger pore volume of 0.266  $\text{cm}^3 \text{g}^{-1}$ . To explore the pore structure, pore size distributions of the OS and POS powders were computed from N<sub>2</sub> adsorption–desorption results (Fig. 10). The OS powders have a narrower pore size distribution than the POS powders. The POS powders have some mesopores (2 nm < pore size < 50 nm), while the OS powders have few. The microporosities of the OS and POS powders are 94 and 74 %, respectively. These results suggest that the OS powders have less porous structures than the POS powders and Pd-doping results in larger and porous microporous structures.

### Membrane characterization

#### Single gas permeance performance

Gas permeances measured with different gases (He, H<sub>2</sub>, CO<sub>2</sub>, N<sub>2</sub>, CH<sub>4</sub>, and SF<sub>6</sub>) at 200 °C are shown in Fig. 11. The POS membrane has higher gas

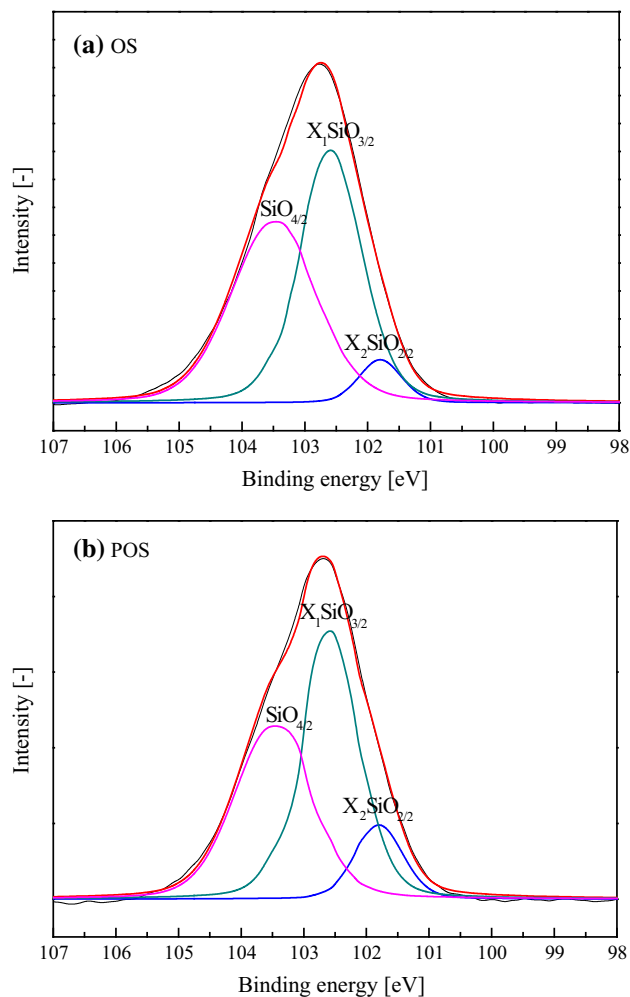


**Figure 8** Deconvolutions of the XPS Si<sub>2p</sub> peaks of the organosilica (OS) (a) and Pd-doped organosilica (POS) (b) powders.

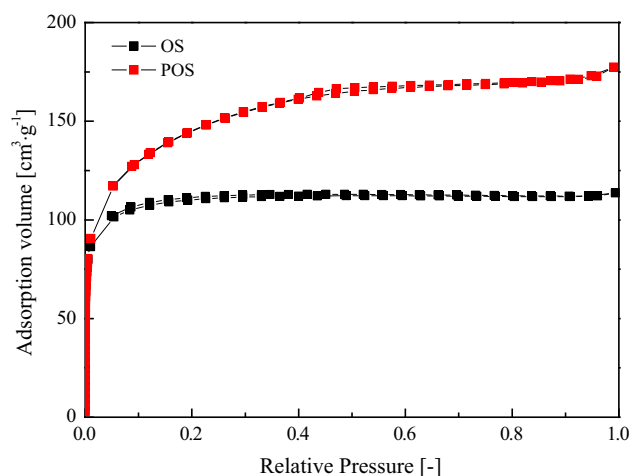


**Figure 9** Nitrogen adsorption–desorption isotherms of the organosilica (OS) and Pd-doped organosilica (POS) powders calcined at 400 °C.

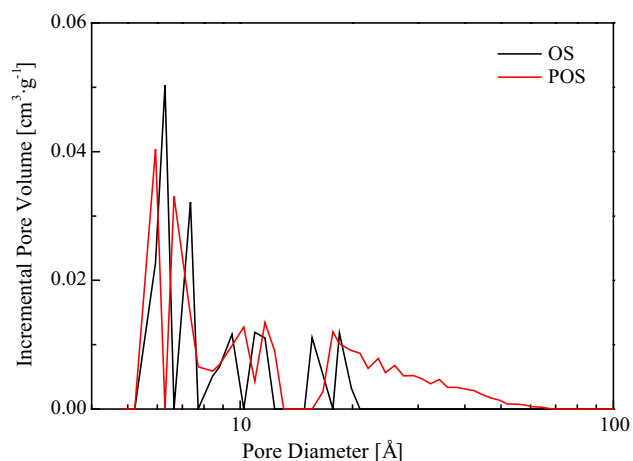


**Figure 10** Pore size distribution of the organosilica (OS) and Pd-doped organosilica (POS) powders calcined at 400 °C.

permeances than the OS membrane. For example, the H<sub>2</sub> permeance of the POS membrane is  $7.26 \times 10^{-7} \text{ mol m}^{-2} \text{ s}^{-1} \text{ Pa}^{-1}$ , while the H<sub>2</sub> permeance of the OS membrane is  $3.75 \times 10^{-7} \text{ mol m}^{-2} \text{ s}^{-1} \text{ Pa}^{-1}$ . The POS membrane has a moderate H<sub>2</sub>/CO<sub>2</sub> ideal selectivity of 4.3, which is close to the Knudsen diffusion factor (4.7 for H<sub>2</sub>/CO<sub>2</sub>), while the OS membrane shows a much higher H<sub>2</sub>/CO<sub>2</sub> separation factor (7.3).

The OS membrane was impermeable to SF<sub>6</sub> gas molecules, indicating the OS membrane has the ultramicropore structure with a pore size smaller than the 0.55 nm diameter of SF<sub>6</sub>. A SF<sub>6</sub> gas permeance of  $1.69 \times 10^{-9} \text{ mol m}^{-2} \text{ s}^{-1} \text{ Pa}^{-1}$  was detected for the POS membrane, suggesting that the POS membrane contains some pores larger than 0.55 nm. The H<sub>2</sub>/SF<sub>6</sub> permselectivity is remarkably high, up to 430, much higher than the corresponding Knudsen diffusion factor of 8.54. This result demonstrates excellent molecular sieving properties of the POS membrane.

These results indicate that Pd-doping has significant effects on the microporous structure of the organosilica membrane. Less microporous structures with larger pores were obtained after doping Pd into the organosilica matrix. This result is in agreement with the gas adsorption isotherm data (Figs. 9, 10).

Apart from the larger pore size after Pd-doping, the higher gas permeances of the POS membrane may also be attributed to the interactions between the Pd and gases. It is well known that Pd and H<sub>2</sub> can have chemical reactions and form Pd-Hydrides. Such chemical interactions (adsorptions) are confirmed by the gas adsorption isotherms of the organosilica (OS) and Pd-doped organosilica (POS) powders (Fig. 12).

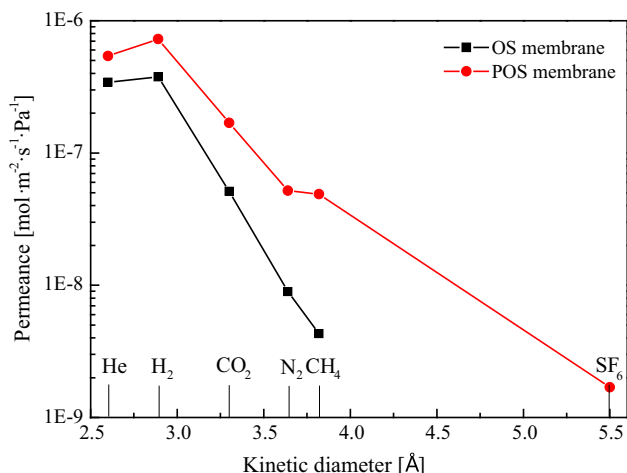


**Figure 11** Single gas permeances of the organosilica (OS) and Pd-doped organosilica (POS) membranes measured at 200 °C.

The dramatically increased H<sub>2</sub> adsorption isotherms of the Pd-doped membrane at low absolute pressures suggest that the H<sub>2</sub> adsorption is caused by chemical interactions. Both OS and POS membranes exhibit slightly increased adsorption isotherms for the other gases (CO<sub>2</sub> and CH<sub>4</sub>) with the increase of the absolute pressure, indicating that their adsorptions result from physical interactions rather than chemical reactions.

Additionally, the approximate pore sizes of the OS and POS membranes may be estimated by the normalized Knudsen-based permeance (NKP) method [42]. In the calculation,  $f_{\text{NKP}}$  is the ratio of the experimental data divided by the ideal Knudsen permeance based on the permeance of standard gas (e.g., H<sub>2</sub> in this work):

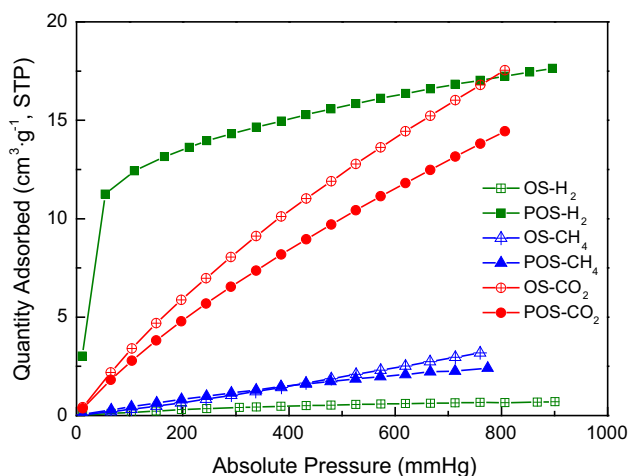


**Figure 12** Gas adsorption isotherms of the organosilica (OS) and Pd-doped organosilica (POS) powders at 298 K.

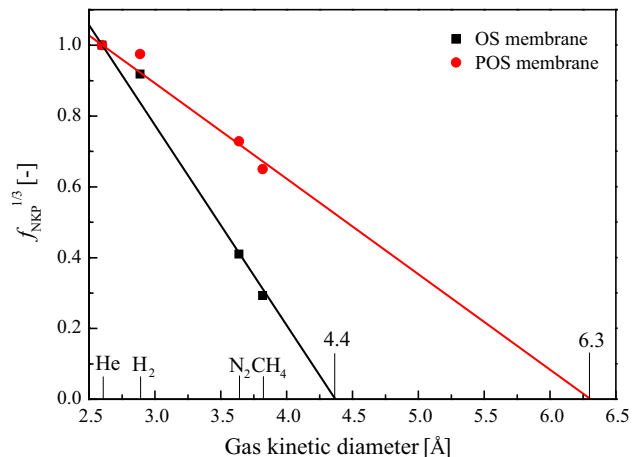


**Figure 13** Relationship between the normalized Knudsen-based permeances ( $f_{\text{NKP}}$ ) and the gas kinetic diameters.

$$f_{\text{NKP}}^{1/3} = \frac{d_p - d_{k,i}}{d_p - d_{k,\text{H}_2}} \quad (1)$$

where  $d_{k,i}$  represents the kinetic diameter of  $i$ th gas,  $d_{k,\text{H}_2}$  represents the kinetic diameter of H<sub>2</sub>, and  $d_p$  is the mean effective pore size of the membrane.

The cube root of  $f_{\text{NKP}}$  as a function of kinetic diameters was linearly fitted with the NKP Eq. (1) and the value of pore size was equal to the x-intercept in the linear fitting equation (Fig. 13). The calculated pore sizes are 0.42 and 0.57 nm for the OS and POS membranes, respectively (Table 1). These values further confirm that the POS membrane has larger pore size after Pd-doping. The pore sizes calculated from the N<sub>2</sub> adsorption–desorption isotherms also indicate the larger pore size of the POS membrane (Table 1). Compared with the pore sizes determined from gas adsorption isotherms, the pore sizes obtained from gas permeation measurements are smaller. Such difference may be caused by the measurement objects (i.e., powders and membranes). The pore sizes determined from the membrane gas permeation measurements are anticipated to be closer to the real ones.

**Table 1** The pore sizes of the membranes obtained from gas adsorption–desorption isotherms and gas permeation measurements

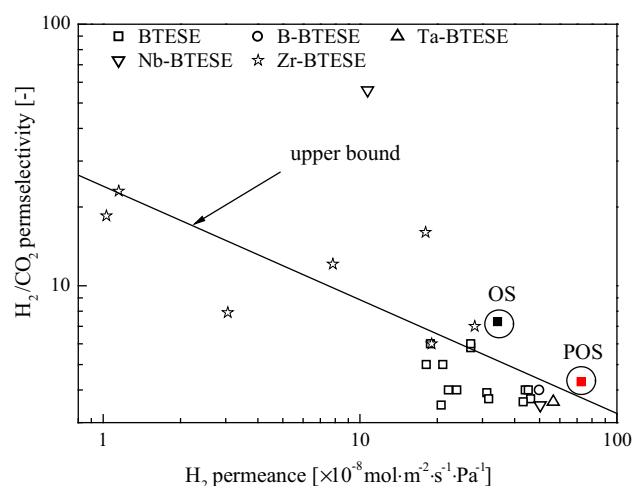
Membrane	Pore size (nm)	
	By N <sub>2</sub> adsorption–desorption isotherms	By gas permeation measurement
OS	0.72	0.42
POS	0.76	0.57

Table 2 and Fig. 14 present the performance comparison in terms of the single gas permeance and permselectivity of OS, POS, and other doped organosilica membranes [31, 33, 37, 43, 44]. The POS membrane in the current work exhibits a much better gas permeability but lower permselectivities compared with Nb- and Zr-doped organosilica membrane [33, 37, 44]. However, the gas permeances and permselectivities of the POS membrane are higher than those of the Nb-, Ta-, and B-doped organosilica membranes [43]. The H<sub>2</sub>/CO<sub>2</sub> separation performances of the OS and POS membranes are beyond the Robeson upper bound (Fig. 14).

*Hydrothermal stability evaluation*

The hydrothermal stabilities of the OS and POS membranes are described in Fig. 15. The H<sub>2</sub> permeance of the OS membrane gradually decreases in the first 74 h, and the CO<sub>2</sub> permeance drops similarly during the first 64 h. This phenomenon is attributed to pore closure caused by the condensation of mobile silanol groups in the smaller pores. After that, the H<sub>2</sub> and CO<sub>2</sub> permeances increase gradually. The increase in gas permeances can be explained by pore widening due to the loss of mobile silica groups. The pore structure of the OS membrane was seriously damaged after continuous hydrothermal treatment for 142 h, which was proved by the significantly increased gas permeances observed after 142 h (Fig. 15).

Compared with the OS membrane, the POS membrane shows relatively stable gas permeances during the 135-h hydrothermal treatment. The CO<sub>2</sub> permeance is 1.69–1.97 × 10<sup>-7</sup> mol m<sup>-2</sup> s<sup>-1</sup> Pa<sup>-1</sup> and the H<sub>2</sub>



**Figure 14** Performance comparison of the organosilica (OS) membranes, Pd-doped organosilica (POS) membranes, and other doped organosilica membranes.

permeance shows a slight increase from 7.29 × 10<sup>-7</sup> to 9.18 × 10<sup>-7</sup> mol m<sup>-2</sup> s<sup>-1</sup> Pa<sup>-1</sup> after 124 h. These results suggest that the micropores allowing H<sub>2</sub> to permeate through slightly increase but they still do not allow CO<sub>2</sub> to permeate through, leading to an enhanced permselectivity. This phenomenon is likely caused by the loss of mobile silica groups in the steam treatment.

After the hydrothermal test, the OS membrane shows a decline in permselectivity of H<sub>2</sub>/CO<sub>2</sub> (from 7.3 to 6.1), while the POS membrane exhibits a slight increase in permselectivity of H<sub>2</sub>/CO<sub>2</sub> (from 4.3 to 5.2), suggesting that the hydrothermal stability of the membrane can be effectively enhanced after Pd-doping.

**Table 2** Performance comparison of the organosilica membranes, Pd-doped organosilica membranes, and other doped organosilica membranes

Membrane materials	Permeance (×10 <sup>-8</sup> mol m <sup>-2</sup> s <sup>-1</sup> Pa <sup>-1</sup> )						Permselectivity		
	He	H <sub>2</sub>	CO <sub>2</sub>	N <sub>2</sub>	CH <sub>4</sub>	SF <sub>6</sub>	H <sub>2</sub> /CO <sub>2</sub>	H <sub>2</sub> /N <sub>2</sub>	H <sub>2</sub> /CH <sub>4</sub>
BTESE [31]	33.2	46.2	12.4	4.4	4	<sup>a</sup>	3.7	10.5	11.5
Nb-BTESE [43]	39.2	50.3	14.3	7.7	4.2	<sup>a</sup>	3.5	6.5	12
B-BTESE [43]	38.8	49.8	12.4	4.3	3.9	0.1	4	11.5	12.7
Ta-BTESE [43]	40.6	56.5	15.6	8.1	4.6	<sup>a</sup>	3.6	7	12.3
Zr-BTESE [33]	N/A	18	1.13	0.18	0.05	N/A	16	100	400
Nb-BTESE [37]	9.4	10.7	0.19	0.13	0.05	<sup>a</sup>	56	82	214
BTESE (this work)	34.3	37.5	5.12	0.89	0.43	<sup>a</sup>	7.3	42	87
Pd-BTESE (this work)	54.1	72.6	16.9	5.18	4.88	0.17	4.3	14	15

N/A relevant data are not available

<sup>a</sup> Gas permeance is below the detection limit of the equipment

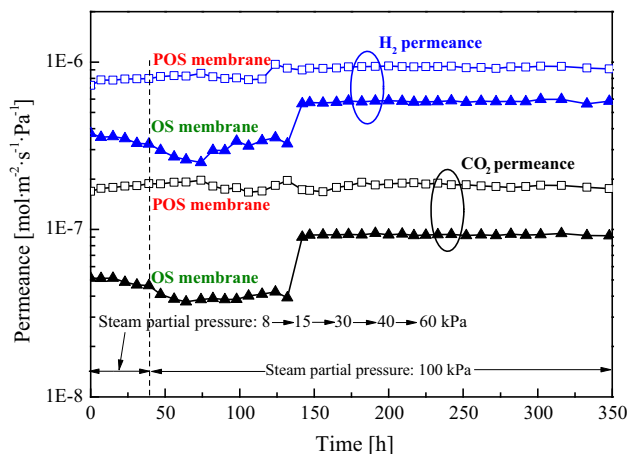


**Figure 15** Comparison of the gas permeances of the organosilica (OS) membrane and Pd-doped organosilica (POS) membrane after steam treatment.

Metal-doping gives a robust M–O–Si structure, resulting in improved hydrothermal stability under steam [19, 45]. In this work, Pd particles were well dispersed in the organosilica matrix (Fig. 6) rather than incorporated into the network of the organosilica. Pd acts as an inhibitor, preventing the breakdown of the network structures of the membrane under steam. This mechanism is similar to the carbon templates in carbonized-template molecular sieve silica [16].

## Conclusions

A Pd-doped organosilica membrane based on BTESE is successfully prepared by the polymeric sol–gel method. TEM, FTIR, and XPS results demonstrate that Pd particles with diameters of 3–10 nm are randomly dispersed in the homogenous organosilica layer instead of being incorporated into the network architectures. Gas adsorption analysis indicates that the Pd-doped organosilica membrane has larger micropores compared with the undoped organosilica membrane.

The separation performance of the Pd-doped membrane in terms of gas permeance, permselectivity, and hydrothermal stability was compared with that of the undoped organosilica membrane. The Pd-doped organosilica membrane has much higher gas permeances than the undoped organosilica membrane ( $7.26$  vs.  $3.75 \times 10^{-7} \text{ mol m}^{-2} \text{ s}^{-1} \text{ Pa}^{-1}$  for  $\text{H}_2$  at  $200^\circ\text{C}$ ) due to the enlarged micropores after Pd-doping. The Pd-doped silica membrane also exhibits a significantly improved hydrothermal stability. The enhanced

hydrothermal stability can be explained by the mechanism that Pd particles act as inhibitors and prevent the formation of mobile silica groups (e.g., Si–OH) under steam. Metal-doping (e.g., Pd-doping in this work) offers a new approach to develop high performance membranes with enhanced gas permeances and hydrothermal stabilities for gas separations.

## Acknowledgements

This work is supported by the National Natural Science Foundation of China (21276123, 21490581), the National High Technology Research and Development Program of China (2012AA03A606), and the “Summit of the Six Top Talents” Program of Jiangsu Province.

## References

- [1] Bernardo P, Drioli E, Golemme G (2009) Membrane gas separation: a review/state of the art. *Ind Eng Chem Res* 48:4638–4663. doi:10.1021/ie8019032
- [2] Baker RW (2002) Future directions of membrane gas separation technology. *Ind Eng Chem Res* 41:1393–1411. doi:10.1021/ie0108088
- [3] Ockwig NW, Nenoff TM (2007) Membranes for hydrogen separation. *Chem Rev* 107:4078–4110. doi:10.1021/cr0501792
- [4] Gabelman A, Hwang S-T (1999) Hollow fiber membrane contactors. *J Membr Sci* 159:61–106. doi:10.1016/s0376-7388(99)00040-x
- [5] Luis P, Van Gerven T, Van der Bruggen B (2012) Recent developments in membrane-based technologies for  $\text{CO}_2$  capture. *Prog Energy Combust Sci* 38:419–448. doi:10.1016/j.peccs.2012.01.004
- [6] Adhikari S, Fernando S (2006) Hydrogen membrane separation techniques. *Ind Eng Chem Res* 45:875–881. doi:10.1021/ie0506441
- [7] Scholes CA, Smith KH, Kentish SE, Stevens GW (2010)  $\text{CO}_2$  capture from pre-combustion processes—strategies for membrane gas separation. *Int J Greenhouse Gas Control* 4:739–755. doi:10.1016/j.ijggc.2010.04.001
- [8] Dong J, Lin YS, Kanazashi M, Tang Z (2008) Microporous inorganic membranes for high temperature hydrogen purification. *J Appl Phys* 104:121301–121317. doi:10.1063/1.3041061
- [9] de Vos RM, Verweij H (1998) High-selectivity, high-flux silica membranes for gas separation. *Science* 279:1710–1711. doi:10.1126/science.279.53537.1710

- [10] Kanezashi M, Sasaki T, Tawarayama H et al. (2014) Experimental and theoretical study on small gas permeation properties through amorphous silica membranes fabricated at different temperatures. *J Phys Chem C* 118:20323–20331. doi:10.1021/jp504937t
- [11] Gallucci F, Fernandez E, Corengia P, Annaland MV (2013) Recent advances on membranes and membrane reactors for hydrogen production. *Chem Eng Sci* 92:40–66. doi:10.1016/j.ces.2013.01.008
- [12] Pera-Titus M (2014) Porous inorganic membranes for CO<sub>2</sub> capture: present and prospects. *Chem Rev* 114:1413–1492. doi:10.1021/cr400237k
- [13] Tsuru T (2008) Nano/subnano-tuning of porous ceramic membranes for molecular separation. *J Sol–Gel Sci Technol* 46:349–361. doi:10.1007/s10971-008-1712-5
- [14] Imai H, Morimoto H, Tominaga A, Hirashima H (1997) Structural changes in sol–gel derived SiO<sub>2</sub> and TiO<sub>2</sub> films by exposure to water vapor. *J Sol–Gel Sci Technol* 10:45–54. doi:10.1023/a:1018332221696
- [15] Castricum HL, Sah A, Kreiter R, Blank DHA, Vente JF, ten Elshof JE (2008) Hybrid ceramic nanosieves: stabilizing nanopores with organic links. *Chem Commun*. doi:10.1039/b718082a
- [16] Duke MC, da Costa JCD, Do DD, Gray PG, Lu GQ (2006) Hydrothermally robust molecular sieve silica for wet gas separation. *Adv Funct Mater* 16:1215–1220. doi:10.1002/adfm.200500456
- [17] Castricum HL, Mittelmeijer-Hazeleger MC, Sah A, ten Elshof JE (2006) Increasing the hydrothermal stability of mesoporous SiO<sub>2</sub> with methylchlorosilanes—a ‘structural’ study. *Microporous Mesoporous Mater* 88:63–71. doi:10.1016/j.micromeso.2005.08.033
- [18] Wei Q, Wang YL, Nie ZR et al. (2008) Facile synthesis of hydrophobic microporous silica membranes and their resistance to humid atmosphere. *Microporous Mesoporous Mater* 111:97–103. doi:10.1016/j.micromeso.2007.07.016
- [19] Boffa V, Blank DHA, ten Elshof JE (2008) Hydrothermal stability of microporous silica and niobia–silica membranes. *J Membr Sci* 319:256–263. doi:10.1016/j.memsci.2008.03.042
- [20] Gu YF, Hacırlıoğlu P, Oyama ST (2008) Hydrothermally stable silica-alumina composite membranes for hydrogen separation. *J Membr Sci* 310:28–37. doi:10.1016/j.memsci.2007.10.025
- [21] Gu YF, Oyama ST (2009) Permeation properties and hydrothermal stability of silica-titania membranes supported on porous alumina substrates. *J Membr Sci* 345:267–275. doi:10.1016/j.memsci.2009.09.009
- [22] Igi R, Yoshioka T, Ikuhara YH, Iwamoto Y, Tsuru T (2008) Characterization of Co-doped silica for improved hydrothermal stability and application to hydrogen separation membranes at high temperatures. *J Am Ceram Soc* 91:2975–2981. doi:10.1111/j.1551-2916.2008.02563.x
- [23] Kanezashi M, Asaeda M (2006) Hydrogen permeation characteristics and stability of Ni-doped silica membranes in steam at high temperature. *J Membr Sci* 271:86–93. doi:10.1016/j.memsci.2005.07.011
- [24] Yoshida K, Hirano Y, Fujii H, Tsuru T, Asaeda M (2001) Hydrothermal stability and performance of silica–zirconia membranes for hydrogen separation in hydrothermal conditions. *J Chem Eng Jpn* 34:523–530. doi:10.1252/jcej.34.523
- [25] Kanezashi M, Yada K, Yoshioka T, Tsuru T (2010) Organic–inorganic hybrid silica membranes with controlled silica network size: preparation and gas permeation characteristics. *J Membr Sci* 348:310–318. doi:10.1016/j.memsci.2009.11.014
- [26] Ren X, Nishimoto K, Kanezashi M, Nagasawa H, Yoshioka T, Tsuru T (2014) CO<sub>2</sub> permeation through hybrid organosilica membranes in the presence of water vapor. *Ind Eng Chem Res* 53:6113–6120. doi:10.1021/ie404386r
- [27] Agirre I, Arias PL, Castricum HL et al. (2014) Hybrid organosilica membranes and processes: status and outlook. *Sep Purif Technol* 121:2–12. doi:10.1016/j.seppur.2013.08.003
- [28] Castricum HL, Paradis GG, Mittelmeijer-Hazeleger MC, Kreiter R, Vente JF, ten Elshof JE (2011) Tailoring the separation behavior of hybrid organosilica membranes by adjusting the structure of the organic bridging group. *Adv Funct Mater* 21:2319–2329. doi:10.1002/adfm.201002361
- [29] Xu R, Ibrahim SM, Kanezashi M et al. (2014) New insights into the microstructure-separation properties of organosilica membranes with ethane, ethylene, and acetylene bridges. *ACS Appl Mater Interfaces* 6:9357–9364. doi:10.1021/am501731d
- [30] Castricum HL, Qureshi HF, Nijmeijer A, Winnubst L (2015) Hybrid silica membranes with enhanced hydrogen and CO<sub>2</sub> separation properties. *J Membr Sci* 488:121–128. doi:10.1016/j.memsci.2015.03.084
- [31] Qureshi HF, Nijmeijer A, Winnubst L (2013) Influence of sol–gel process parameters on the micro-structure and performance of hybrid silica membranes. *J Membr Sci* 446:19–25. doi:10.1016/j.memsci.2013.06.024
- [32] Qi H, Chen HR, Li L, Zhu GZ, Xu NP (2012) Effect of Nb content on hydrothermal stability of a novel ethylene-bridged silsesquioxane molecular sieving membrane for H<sub>2</sub>/CO<sub>2</sub> separation. *J Membr Sci* 421:190–200. doi:10.1016/j.memsci.2012.07.010
- [33] ten Hove M, Nijmeijer A, Winnubst L (2015) Facile synthesis of zirconia doped hybrid organic inorganic silica membranes. *Sep Purif Technol* 147:372–378. doi:10.1016/j.seppur.2014.12.033

- [34] Kanezashi M, Sano M, Yoshioka T, Tsuru T (2010) Extremely thin Pd–silica mixed-matrix membranes with nano-dispersion for improved hydrogen permeability. *Chem Commun* 46:6171–6173. doi:[10.1039/C0CC01461C](https://doi.org/10.1039/C0CC01461C)
- [35] Liu L, Wang DK, Martens DL, Smart S, da Costa JCD (2015) Influence of sol-gel conditioning on the cobalt phase and the hydrothermal stability of cobalt oxide silica membranes. *J Membr Sci* 475:425–431. doi:[10.1016/j.memsci.2014.10.037](https://doi.org/10.1016/j.memsci.2014.10.037)
- [36] Kanezashi M, Miyauchi S, Nagasawa H, Yoshioka T, Tsuru T (2014) Gas permeation properties through Al-doped organosilica membranes with controlled network size. *J Membr Sci* 466:246–252. doi:[10.1016/j.memsci.2014.04.051](https://doi.org/10.1016/j.memsci.2014.04.051)
- [37] Qi H, Han J, Xu NP (2011) Effect of calcination temperature on carbon dioxide separation properties of a novel microporous hybrid silica membrane. *J Membr Sci* 382:231–237. doi:[10.1016/j.memsci.2011.08.013](https://doi.org/10.1016/j.memsci.2011.08.013)
- [38] Uhlmann D, Liu S, Ladewig BP, Diniz da Costa JC (2009) Cobalt-doped silica membranes for gas separation. *J Membr Sci* 326:316–321. doi:[10.1016/j.memsci.2008.10.015](https://doi.org/10.1016/j.memsci.2008.10.015)
- [39] Ngamou PHT, Overbeek JP, Kreiter R et al. (2013) Plasma-deposited hybrid silica membranes with a controlled retention of organic bridges. *J Mater Chem A* 1:5567–5576. doi:[10.1039/c3ta00120b](https://doi.org/10.1039/c3ta00120b)
- [40] Yamamoto K, Ohshita J, Mizumo T, Tsuru T (2015) Efficient synthesis of SiOC glasses from ethane, ethylene, and acetylene-bridged polysilsesquioxanes. *J Non-Cryst Solids* 408:137–141. doi:[10.1016/j.jnoncrsol.2014.10.024](https://doi.org/10.1016/j.jnoncrsol.2014.10.024)
- [41] da Costa JCD, Lu GQ, Rudolph V (2001) Characterisation of templated xerogels for molecular sieve application. *Colloid Surf A Physicochem Eng Asp* 179:243–251. doi:[10.1016/S0927-7757\(00\)00644-0](https://doi.org/10.1016/S0927-7757(00)00644-0)
- [42] Lee HR, Kanezashi M, Shimomura Y, Yoshioka T, Tsuru T (2011) Evaluation and fabrication of pore-size-tuned silica membranes with tetraethoxydimethyl disiloxane for gas separation. *AIChE J* 57:2755–2765. doi:[10.1002/aic.12501](https://doi.org/10.1002/aic.12501)
- [43] Qureshi HF, Besselink R, ten Elshof JE, Nijmeijer A, Winubst L (2015) Doped microporous hybrid silica membranes for gas separation. *J Sol–Gel Sci Technol* 75:180–188. doi:[10.1007/s10971-015-3687-3](https://doi.org/10.1007/s10971-015-3687-3)
- [44] Song H, Zhao S, Chen J, Qi H (2016) Hydrothermally stable Zr-doped organosilica membranes for H<sub>2</sub>/CO<sub>2</sub> separation. *Microporous Mesoporous Mater* 224:277–284. doi:[10.1016/j.micromeso.2016.01.001](https://doi.org/10.1016/j.micromeso.2016.01.001)
- [45] Castricum HL, Sah A, Kreiter R, Blank DHA, Vente JF, ten Elshof JE (2008) Hydrothermally stable molecular separation membranes from organically linked silica. *J Mater Chem* 18:2150–2158. doi:[10.1039/b801972j](https://doi.org/10.1039/b801972j)